

# The Scaling Behaviour of a Turbulent Kinetic Energy Closure Model for Stably Stratified Conditions

Peter Baas · Stephan R. de Roode · Geert Lenderink

Received: 9 March 2007 / Accepted: 27 November 2007  
© Springer Science+Business Media B.V. 2007

**Abstract** We investigate the scaling behaviour of a turbulent kinetic energy (TKE) closure model for stably stratified conditions. The mixing length scale for stable stratification is proportional to the ratio of the square root of the TKE and the local Brunt–Väisälä frequency, which is a commonly applied formulation. We analyze the scaling behaviour of our model in terms of traditional Monin–Obukhov Similarity Theory and local scaling. From the model equations, we derive expressions for the stable limit behaviour of the flux–gradient relations and other scaling quantities. It turns out that the scaling behaviour depends on only a few model parameters and that the results obey local scaling theory. The analytical findings are illustrated with model simulations for the second GABLS intercomparison study. We also investigate solutions for the case in which an empirical correction function is used to express the eddy diffusivity for momentum as a function of the Richardson number (i.e. an increasing turbulent Prandtl number with stability). In this case, it seems that for certain parameter combinations the model cannot generate a steady-state solution. At the same time, its scaling behaviour becomes unrealistic. This shows that the inclusion of empirical correction functions may have large and undesired consequences for the model behaviour.

**Keywords** Closure model · Monin–Obukhov Similarity Theory · Parameterization · Stable boundary layer · Turbulent kinetic energy

## 1 Introduction

Turbulent motions transport momentum, heat and trace gases vertically through the boundary layer, which forms the connection between the earth's surface and the free atmosphere. A proper modelling of these exchange processes is of vital importance for accurate numerical weather prediction (NWP) and climate modelling (Weng and Taylor 2003). Despite decennia

---

P. Baas (✉) · S. R. de Roode · G. Lenderink  
Regional Climate Section, Royal Netherlands Meteorological Institute, Wilhelminalaan 10, P.O. Box 201,  
3730 AE, De Bilt, The Netherlands  
e-mail: peter.baas@knmi.nl

of research, modelling turbulent motions in a satisfactory way is still challenging, especially in the stable boundary layer (Holtslag 2006). Here mechanisms such as radiation divergence, slope flows, gravity waves and an increased sensitivity to surface heterogeneity add complications for the flow description (Mahrt et al. 1998). To account for turbulent motions, in many atmospheric models Reynolds decomposition is applied, which involves separation of the flow into a mean part and a turbulent or subgrid part. As a result, every prognostic equation for a mean variable contains at least one unknown turbulence flux term. This problem is known as the closure problem (e.g. Stull 1988).

A commonly applied method to close the system is the eddy-diffusivity approach, where the vertical turbulent flux  $\overline{w'\psi'}$  is taken proportionally to an eddy diffusivity,  $K_\psi$ , and the vertical gradient of the mean value of the variable  $\psi$ :

$$\overline{w'\psi'} = -K_\psi \frac{\partial \overline{\psi}}{\partial z}. \quad (1)$$

Often  $K_\psi$  is expressed as a function of stability by applying semi-empirical stability functions (e.g. Holtslag 1998), and because only the equations for the mean variables are solved, this method is called first-order closure.

In a more advanced approach,  $K_\psi$  can be made a function of the turbulence itself. This turbulent kinetic energy (TKE) closure accounts better for the turbulent character of the flow (e.g. Basu et al. 1998) and is termed 1.5-order closure. Besides prognostic equations for the mean quantities, TKE-closure models also contain a prognostic equation for TKE. In TKE- $l$  models the eddy diffusivities depend on TKE (or  $E$ ) and a diagnostic length scale,  $l_\psi$ :

$$K_\psi = l_\psi \sqrt{E}. \quad (2)$$

The closure problem now consists of finding appropriate expressions for the length scale, yet to date no consensus exists on how to model this quantity. Many different forms are proposed in the literature, often based on simple physical concepts and/or ad-hoc matching arguments (Bougeault and Lacarrère 1989; Brinkop and Roeckner 1995; Cuxart et al. 2000; Lenderink and Holtslag 2004; henceforth LH04).

In principle, much more complex closure models can be derived (see, for an overview, Weng and Taylor 2003; Umlauf and Burchard 2005). Relatively simple 1.5- and second-order closure models based on the work of Mellor and Yamada (1974) are frequently applied. By comparing model output with large-eddy simulation data, Canuto et al. (2001) and Cheng et al. (2002) point to deficiencies of this type of model. They propose improved closure schemes by adding more advanced physics. However, even the implementation of 1.5-order or ordinary second-order closure models in NWP models is often rather complex. Practical difficulties involve the numerics (instability), constraints due to the computational costs (complexity, timestep and resolution), and the requirement to have robust behaviour over the full range of atmospheric conditions (see e.g. Lenderink et al. 2004). It is therefore questionable whether more advanced physics outweighs the potentially less robustness of such complex models (Weng and Taylor 2003).

In this study we make use of the single column version of the Regional Atmospheric Climate Model (RACMO2), in operation at KNMI (Lenderink et al. 2003). A TKE scheme was implemented in this model, in particular to improve the representation of cloudy boundary layers. Here we study consequences for the stable boundary layer. Recent intercomparison studies have shown that in stable conditions TKE models perform well compared to first-order closure research models (Cuxart et al. 2006; Steeneveld et al. 2007). However, the scaling behaviour of TKE models has received little attention in the literature. For example,

it is not clear to what extent such models obey well-established Monin–Obukhov Similarity Theory (MOST), especially on a relatively coarse vertical grid resolution.

This study investigates the stable boundary layer (SBL) scaling behaviour of a TKE-*l* scheme with a commonly used length scale in terms of traditional MOST and local scaling. In particular, it is questioned whether this behaviour is realistic and to what extent it can be controlled. To put it differently, we want to establish how TKE closure relates to the more simple first-order closure. Section 2 provides some background on MOST and model closure. In Sect. 3 the TKE scheme is described, and starting from the model equations, in Sect. 4 we derive expressions for the stable limit of the flux–gradient relations. Section 5 illustrates the analytical findings with model integrations for the second GEWEX Atmospheric Boundary Layer Studies (GABLS; [Holtslag 2006](#)) intercomparison case. The results are compared with scaling relations obtained from observations. It will be argued that our model can be considered a reduced version of the full second-order [Nieuwstadt \(1984\)](#) model. To see how the simplifications affect the model’s scaling behaviour we compare some of our results with those of [Nieuwstadt \(1984\)](#). After discussing the results in Sect. 6, the conclusions are summarized in Sect. 7.

## 2 Background

In first-order closure models,  $K$  is often expressed as (e.g. [Duykerke 1991](#); [Holtslag 1998](#)):

$$K_{\psi} = l^2 \left| \frac{\partial \vec{V}}{\partial z} \right| F_{\psi} (Ri_g), \tag{3}$$

where  $l$  is a mixing length, and, for example, in near neutral conditions is expressed as  $\kappa z$ .  $F_{\psi}$  is a correction function that accounts for effects of stratification, depending on the gradient Richardson number,  $Ri_g$ ,

$$Ri_g = \frac{\left(\frac{g}{\theta_v}\right) \frac{\partial \overline{\theta_v}}{\partial z}}{\left(\frac{\partial \overline{u}}{\partial z}\right)^2 + \left(\frac{\partial \overline{v}}{\partial z}\right)^2}. \tag{4}$$

The shape of  $F_{\psi}$  can be obtained by using similarity theory. We focus on the local scaling theory of [Nieuwstadt \(1984\)](#), which can be considered as an extension of the surface-based MOST with local fluxes replacing surface fluxes. According to the local scaling approach, each dimensionless group is a only a function of the stability parameter  $z/\Lambda$ ,

$$\frac{z}{\Lambda} = \zeta = \frac{-\kappa z \frac{g}{\theta_v} \overline{w'\theta_v'}}{u_*^3}, \tag{5}$$

where  $\Lambda$  is the local Obukhov length,  $u_*$  is the friction velocity and  $\overline{w'\theta_v'}$  is the virtual potential temperature flux. The dimensionless shear,  $\phi_m$  (Eq. 6) and the dimensionless virtual potential temperature gradient,  $\phi_h$  (Eq. 7) are defined by

$$\phi_m (\zeta) = \frac{\kappa z}{u_*} \left[ (\partial \overline{u} / \partial z)^2 + (\partial \overline{v} / \partial z)^2 \right]^{1/2} \tag{6}$$

and,

$$\phi_h (\zeta) = \left( \frac{\kappa z}{\theta_*} \right) \frac{\partial \overline{\theta_v}}{\partial z}, \tag{7}$$

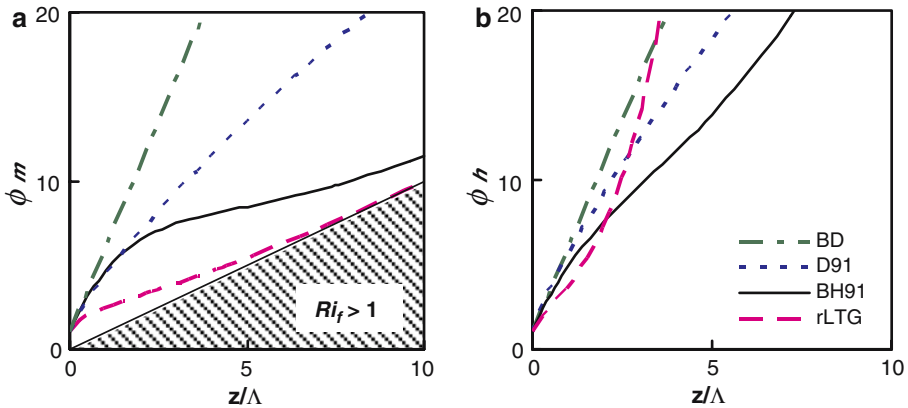


**Fig. 1** Selected flux–gradient relations for momentum (a) and heat (b) from the literature. BD: Businger–Dyer; D91: Duynkerke (1991); BH91: Beljaars and Holtslag (1991); rLTG: revised Louis–Tiedtke–Geleyn, taken from Viterbo et al. (1999)

where  $\theta_* = -\overline{w'\theta'_v}/u_*$  is a turbulent temperature scale and the subscripts  $m$  and  $h$  refer to momentum and heat, respectively. The shape of these flux–gradient relations or  $\phi$  functions must be determined by experiment. For very strong stratification it can be argued that the size of the turbulent eddies is not related to the height above the surface, and therefore,  $z$  drops as a relevant parameter for large values of  $z/\Lambda$ . In this stable limit of local scaling theory the dimensionless gradients become proportional to  $z/\Lambda$ , yielding linear  $\phi$  functions. This regime is referred to as  $z$ -less scaling (Nieuwstadt 1984). A linear interpolation between the neutral and the very stable limit gives  $\phi_{m,h} = 1 + \beta_{m,h}z/\Lambda$  (Zilitinkevich and Esau 2007).

Figure 1 gives some examples of flux–gradient relations that have been proposed in the literature (Businger et al. 1971; Dyer 1974; Duynkerke 1991; Beljaars and Holtslag 1991 (henceforth BH91); Viterbo et al. 1999). We will compare the scaling behaviour of our model with these proposed flux–gradient functions. As will be discussed below, contrary to the other formulations, the revised Louis–Tiedtke–Geleyn (rLTG) functions proposed by Viterbo et al. (1999) are not based on experimental data but on large-scale model performance.

For weakly stable conditions, when turbulence is continuous, most studies agree on the Businger–Dyer functions (Businger et al. 1971; Dyer 1974), which state that  $\phi_m = \phi_h = 1 + 5\zeta$ . However, when  $\zeta$  becomes larger than about 1 the observations start to level off and the proposed formulations diverge (see Höglström 1988; Andreas 2002 for a review). In this regime with very strong stratification turbulence becomes patchy and intermittent (Mahrt et al. 1998), thus violating basic assumptions underlying MOST. This may explain the deviation of the  $\phi$  functions from the linear relation (Cheng et al. 2005). Mahrt (2007) shows that nonstationarity promotes this levelling off of the flux–gradient relations. Note that the  $\phi$  functions are seriously affected by self-correlation because the occurrence of  $u_*$  in both  $z/L$  and  $\phi_m$  and  $\phi_h$  (e.g. Baas et al. 2006).

The following equations relate  $Ri_g$  and the flux-Richardson number,  $Ri_f$  (which is the ratio of the buoyancy destruction and the shear production in the TKE equation) to the flux–gradient relations (see e.g. Duynkerke and de Roode 2001):

$$Ri_g = \zeta \frac{\phi_h}{\phi_m^2}, \tag{8}$$

$$Ri_f = \frac{\zeta}{\phi_m}. \tag{9}$$

The maximum value of  $Ri_f$  is 1, i.e. the buoyancy destruction can never be larger than the shear production. In Fig. 1 the dashed area indicates where this theoretical demand is violated. The functions of both BH91 and rLTG approach  $Ri_f = 1$  in their stable limit. The turbulent Prandtl number,  $Pr$  is defined by

$$Pr = \frac{K_m}{K_h} = \frac{\phi_h}{\phi_m} = \frac{Ri_g}{Ri_f}. \tag{10}$$

The shape of  $F_\psi$  follows directly from the  $\phi$  functions:

$$F_\psi = \frac{1}{\phi_m(\zeta)\phi_\psi(\zeta)}. \tag{11}$$

By Eq. 8  $F_\psi$  becomes a function of  $Ri_g$ . However, when observationally based stability functions (e.g. BH91) are applied in operational models, model performance deteriorates (Beljaars and Viterbo 1998): nighttime minimum temperatures tend to be too low and mid-latitude cyclones tend to become too vigorous. To avoid these problems the stability functions are tuned to obtain optimal model performance: widely used are the rLTG functions proposed by Viterbo et al. (1999), based on work by Louis et al. (1982). It seems that large-scale models need much more mixing than can be motivated by observations from field experiments. Differences between observed mixing characteristics and the mixing that is apparently needed by operational models may be explained by surface heterogeneity (Mahrt 1987; McCabe and Brown 2007) and small-scale gravity wave drag (Chimonas and Nappo 1989). Unfortunately, this so-called ‘enhanced mixing’ severely deteriorates the stable boundary-layer structure. Typically the boundary layer becomes too thick and the low-level jet spreads out with height (Cheng et al. 2005; Cuxart et al. 2006). Implementing a TKE-closure scheme does not solve the problem: good operational model performance and a realistic boundary-layer structure at the same time are still hard to achieve (Jones et al. 2003).

### 3 Model Description

In this section we describe the vertical diffusion scheme of our model for stable stratification. Assuming horizontally homogeneous conditions, the prognostic TKE equation (e.g. Stull 1988) is given by:

$$\frac{\partial E}{\partial t} = - \left( \overline{u'w'} \frac{\partial \bar{u}}{\partial z} + \overline{v'w'} \frac{\partial \bar{v}}{\partial z} \right) + \frac{g}{\theta_v} \overline{w'\theta'_v} - \frac{\partial}{\partial z} \left( \overline{w'E} + \overline{w'p'}/\bar{\rho} \right) - \varepsilon, \tag{12}$$

where the terms on the right-hand side represent production due to the wind shear and the buoyancy, the transport of TKE and the dissipation respectively. These terms are parameterized according to

$$-\left(\overline{u'w'}\frac{\partial\bar{u}}{\partial z} + \overline{v'w'}\frac{\partial\bar{v}}{\partial z}\right) = K_m \left[ \left(\frac{\partial\bar{u}}{\partial z}\right)^2 + \left(\frac{\partial\bar{v}}{\partial z}\right)^2 \right] = K_m S^2, \tag{13a}$$

$$\frac{g}{\theta_v}\overline{w'\theta'_v} = -K_h \frac{g}{\theta_v}\frac{\partial\bar{\theta}_v}{\partial z} = -K_h N^2, \tag{13b}$$

$$-\left(\overline{w'E} + \overline{w'p'}/\bar{\rho}\right) = 2K_m \frac{\partial E}{\partial z}, \tag{13c}$$

$$\varepsilon = c_d \frac{E^{3/2}}{l_m}. \tag{13d}$$

Note the definitions of the Brunt–Väisälä frequency,  $N$  and the vertical wind shear,  $S$ . For stably stratified conditions, the length scale in the model is given by

$$\frac{1}{l_{m,h}} = \frac{1}{c_n \kappa z} + \frac{1}{l_s}, \tag{14}$$

and in the limit of neutral stratification this reduces to  $c_n \kappa z$ . The surface boundary condition for TKE is given by

$$E_{surf} = c_0 u_*^2 + 0.2 w_*^2, \tag{15}$$

where  $c_0 = 3.75$  (Wyngaard and Coté 1971) is an empirical parameter and  $w_*$  is the convective velocity scale, which can be neglected in stable conditions. From a surface-layer matching procedure, LH04 show that  $c_d = c_o^{-2} = 0.0711$ . After correcting for differences in the definition of the length scale used (most constant pre-factors), this value is equivalent to those used in, for example, Cuxart et al. (2000) and Brinkop and Roeckner (1995). In an analogous way Mailot and Benoit (1982) show that the value of  $c_n = 0.516$ . We refer to LH04 for more details. The length scale for stable stratification (Deardorff 1980),

$$l_s = c_{m,h} \frac{\sqrt{E}}{N}, \tag{16}$$

dominates in the very stable regime. The mixing efficiencies  $c_{m,h}$  are model parameters that are not necessarily the same; LH04 take  $c_h = 0.2$  as a reference value. The parameter  $c_h$  not only regulates the vertical diffusion in the stable boundary layer, it also affects the entrainment rate (Brinkop and Roeckner 1995; Lenderink and Holtslag 2000). The optimal value for  $c_h$  seems to vary with boundary-layer regime (Lock and Mailhot 2006).

With increasing stability, it is often argued that momentum is mixed more efficiently than heat, probably due to wave activity (Kondo et al. 1978; Kim and Mahrt 1992). This process is taken into account by expressing Pr as a function of  $Ri_g$  (LH04):

$$c_m = c_h \text{Pr} = c_h(1 + c_p Ri_g). \tag{17}$$

Data presented by Kim and Mahrt (1992) and Schumann and Gerz (1995) suggest a value of  $c_p$  that ranges from 2 to 4. However, other studies, as for example Howell and Sun (1999), do not find a clear dependency of Pr on stability. Note that spurious self-correlation stimulates a positive correlation between Pr and  $Ri_g$ , preventing examination of the physical significance of this relationship (Mahrt 2007). In this study we vary  $c_p$  between 0 and 2. In NWP practice, the values of constants such as  $c_p$  are most often based on optimal model performance rather than on sound values from the laboratory or field experiments. By expressing  $c_m$  as a function of stability, Jones et al. (2003) obtain a large reduction in the root-mean-square and the bias of the mean sea level pressure and the geopotential with a comparable diffusion scheme, implemented in a 3D version of the Hirlam model.

### 4 Analytical Solution for the Stable Limit of the TKE Model

We analyze the scaling behaviour of the model for very strong stratification by deriving expressions for the slope of the  $\phi$  functions from the model equations. For strong stratification, the length scale is determined by  $l_s$  (Eq. 16). Then the eddy diffusivities can be expressed as

$$K_{m,h} = l_s \sqrt{E} = c_{m,h} \frac{E}{N}. \tag{18}$$

Following Eq. 13 the parameterized TKE equation becomes

$$\frac{\partial E}{\partial t} = K_m S^2 - K_h N^2 - c_d \frac{E^{\frac{3}{2}}}{l_m}. \tag{19}$$

In this analytical analysis, we neglect the transport term for simplicity. In Sect. 5, we compare the analytical results with numerical simulations of the TKE model using the complete set of equations. The output shows that for stable conditions the transport term is indeed very small in the model, which justifies this assumption in the context of our model. Although in reality the transport term is generally small in the SBL (e.g. Nieuwstadt 1984), under certain conditions (e.g. intermittency) it can be considerable (Cuxart et al. 2002).

After using the eddy diffusivities (Eq. 18), the length scale (Eq. 16) and using Eqs. 9, 10 and 17, Eq. 19 can be written as

$$\frac{\partial E}{\partial t} = c_h EN \left[ \frac{c_m}{c_h} \frac{1}{Ri_g} - \left( 1 + \frac{c_d}{c_m c_h} \right) \right] = c_h EN \left[ \frac{\phi_m}{\zeta} - \left( 1 + \frac{c_d}{c_m c_h} \right) \right]. \tag{20}$$

In Sect. 4.1 we consider the situation where Pr is constant, and then study the consequences of an increasing Pr with stability in Sect. 4.2. Section 4.3 discusses some complications that arise with the current stability dependency of Pr.

#### 4.1 Pr is Constant

Assuming a stationary state, Eq. 20 leads to a simple expression for the slope of the  $\phi$  functions that only depends on model parameters. In the case that  $c_m$  and  $c_h$  are constants it follows that

$$\frac{\phi_m}{\zeta} = 1 + \frac{c_d}{c_m c_h} \tag{21}$$

and

$$\frac{\phi_h}{\zeta} = \frac{c_m}{c_h} \frac{\phi_m}{\zeta} = \frac{c_m}{c_h} + \frac{c_d}{c_h^2}. \tag{22}$$

Since this equilibrium (stable limit) solution contains just model constants it states that  $\phi_m$  becomes linear with  $\zeta$ , which agrees with the asymptotic limit of local scaling theory ( $z$ -less scaling). Using Eq. 8, the corresponding critical  $Ri_g$  can be expressed as

$$Ri_g = \frac{1}{\frac{c_h}{c_m} + \frac{c_d}{c_m^2}}. \tag{23}$$

For example, if we set  $c_m = c_h = 0.13$  we obtain  $\phi_m = \phi_h = 5\zeta$ , which is the stable limit of the Businger–Dyer relations. The corresponding critical  $Ri_g = 0.2$ .

It should be noted that the concept of a critical  $Ri_g$  (which was often assumed to be about 0.25) is debatable. Numerous experimental studies show turbulent activity at values

of  $Ri_g > 1$  (e.g. Kondo et al. 1978; Kim and Mahrt 1992; Zilitinkevich et al. 2007). Rather than having a strict critical  $Ri_g$  above which a flow is always laminar, a *transition regime* can be identified separating a weakly stable ( $Ri_g < O(0.1)$ ) and a very stable regime ( $Ri_g > O(1)$ ) (see theoretical analysis in Zilitinkevich et al. (2007), and data analysis in op. cit. and Mauritsen and Svensson 2007). In the former regime turbulence is strong and MOST can be applied, contrary to the latter regime where turbulent motions *do* exist but are weak and nonstationair (Mahrt et al. 1998). Bertin et al. (1997) suggest that  $Ri_f$  rather than  $Ri_g$  is the relevant parameter for defining the eddy diffusivity.

#### 4.2 Pr Increases with Stability

To allow for an increasing Pr with stability, we take into account Eq. 17. By using Eq. 10 we can express  $c_m$  (which is no longer a constant) as

$$c_m = c_h (1 + c_p Ri_g) = c_h \left( 1 + c_p \frac{c_m}{c_h} Ri_f \right). \tag{24}$$

Solving for  $c_m$  (and using Eq. 9) gives this parameter in terms of model constants and  $\phi_m/\zeta$ :

$$c_m = \frac{c_h}{\left( 1 - c_p \frac{\zeta}{\phi_m} \right)}. \tag{25}$$

Combining Eqs. 21 and 25 leads to a quadratic equation, with solutions

$$\frac{\phi_m}{\zeta} = \frac{1}{2} \left( 1 + \frac{c_d}{c_h^2} \right) \pm \frac{1}{2} \sqrt{\left( 1 + \frac{c_d}{c_h^2} \right)^2 - 4c_p \frac{c_d}{c_h^2}}. \tag{26}$$

Equation 26 gives the slope of  $\phi_m(\zeta)$  in the stable limit as only a function of  $c_h$  and  $c_p$ . For  $\phi_h$  it can be shown that

$$\frac{\phi_h}{\zeta} = \frac{c_m}{c_h} \frac{\phi_m}{\zeta} = \frac{c_d}{c_h^2} + \frac{1}{\left( 1 - c_p \frac{\zeta}{\phi_m} \right)}. \tag{27}$$

Equations 26 and 27 reduce to Eqs. 21 and 22 for  $c_p = 0$ , providing that  $c_m = c_h$ . The ‘minus-solution’ in Eq. 26 is never followed by the model and has no physical meaning since it causes  $\phi_h/\zeta < 0$  (in most cases), i.e. it requires an unstable stratification in the considered stable limit. Therefore in the following we focus on the ‘plus-solutions’ of Eqs. 26 and 27. Figure 2 presents lines of equal  $\phi_m/\zeta$  and  $\phi_h/\zeta$  as a function of  $c_h$  and  $c_p$ . Regime I indicates the parameter space where the model obeys local scaling theory. In regimes II and III this is not the case: these situations correspond to parameter combinations for which no steady state solution exists or which do not have a physical meaning. These last two regimes are discussed in the next sub-section.

#### 4.3 Comments on the Current Formulation of Pr versus Stability

Due to the dependency of  $c_m$  on  $\phi_m/\zeta$  itself, the relation for  $\phi_m/\zeta$  (Eq. 26) becomes quadratic. Consequently the solution of this equation contains a square root, which can become negative for certain combinations of  $c_h$  and  $c_p$ . It turns out that the system only has a real solution for

$$c_p \leq \frac{1}{2} + \frac{c_d}{4c_h^2} + \frac{c_h^2}{4c_d}. \tag{28}$$

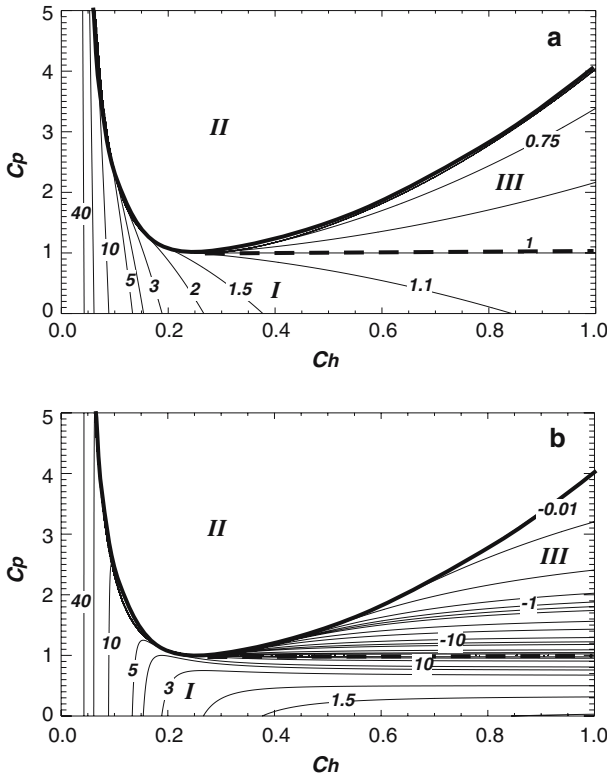


**Fig. 2** Contour plots of  $\phi_m/\zeta$  (a) and  $\phi_h/\zeta$  (b) as a function of  $c_h$  and  $c_p$  following the ‘plus-solutions’ of Eqs. 26 and 27, which indicate the slope of the  $\phi$  functions in the stable limit. In regime I the model obeys local scaling theory. Regime II indicates parameter combinations where no stable limit solution exists. The solutions in regime III have no physical meaning since values for  $\phi_h/\zeta$  are negative and  $\phi_m/\zeta < 1$  ( $Rif > 1$ )

This is indicated in Fig. 2, which separates the real and imaginary solutions of Eq. 25: apparently, in regime II a strictly stable limit solution does not exist.

To obtain more insight in why a parameter range without a real solution exists, we further analyze the stable limit of the TKE equation. By using Eq. 18 for the eddy diffusivities and Eq. 17 for  $c_m$ , the stationary TKE equation (19) can be written as

$$\left[ 1 + c_p \frac{N^2}{S^2} \right] c_h S^2 - c_h N^2 - \frac{c_d}{c_h} \frac{N^2}{\left[ 1 + c_p \frac{N^2}{S^2} \right]} = 0 \tag{29}$$

For increasing  $c_p$  the buoyancy term is unaffected but the shear term becomes larger and the dissipation becomes smaller. It turns out that when  $c_p$  exceeds the threshold value imposed by Eq. 28, the shear term becomes *so* large that the buoyancy destruction and the dissipation cannot balance the shear production anymore, indicating that a steady-state solution is no longer possible and  $\partial E/\partial t > 0$ . Note that the extra shear production scales with the buoyancy destruction. For  $c_p = 1$  the buoyancy destruction is fully compensated by the extra shear production and ‘vanishes’.

A second problem, raised by Eq. 27, is that the value of  $\phi_h/\zeta$  might become negative, and this turns out to be the case in regime III of Fig. 2, when  $c_h > 0.26$  and  $c_p > 1$ . Note that  $\phi_m/\zeta < 1$  in this regime, corresponding to the unphysical  $Ri_f > 1$ .

Equation 29 can be expressed as a quadratic equation in  $Ri_g$ . Solving gives an expression for the critical  $Ri_g$  as a function of only  $c_h$  and  $c_p$ :

$$Ri_g = -\frac{2c_p - 1 - \frac{c_d}{c_h^2}}{2c_p(c_p - 1)} \pm \frac{1}{2c_p(c_p - 1)} \sqrt{\left(1 + \frac{c_d}{c_h^2}\right)^2 - 4c_p \frac{c_d}{c_h^2}}, \tag{30}$$

where only the ‘minus-solution’ gives realistic values. In the case of  $c_p = 0$ , Eq. 29 simply reduces to Eq. 23. Also for  $c_p = 1$ , Eq. 29 reduces to a linear equation. Values for the critical  $Ri_g$  can be obtained by taking the limit of  $c_p \rightarrow 1$  in Eq. 30 as well.

### 5 Comparison of the Analytical Solutions with Model Simulations of the TKE Model

We compare the analytical solutions for the stable limit (obtained in Sect. 4) with model simulations of the full TKE model (Sect. 3) for the second GABLS intercomparison study (Svensson and Holtslag 2006). This case is based on observations from the CASES-99 measurement campaign (Poulos et al. 2002), which was organized in October 1999 in Kansas, U.S.A (37.65°N, 96.74°W; 440 m a.s.l.). A constant geostrophic forcing is applied and the surface temperature is prescribed as a function of time. The simulation time is 59 h, starting at 1400 local time and we use a high vertical resolution of about 5 m. The timestep is 300 s. For our analysis we only use model output from the lowest 40 levels, i.e. below 200 m. Because it is often argued that the results of TKE models depend relatively strongly on vertical resolution we also performed some runs on low resolution. When the number of levels is reduced to 60 (one level about each 40 m close to the surface) exactly the same scaling results are obtained, indicating that the conclusions are also applicable for operational resolutions. Also the vertical wind profiles of the low resolution runs give similar results as the ones with high resolution. We stress that we focus on the scaling behaviour of the model and not on simulating the observations. For such a study we refer to Steeneveld et al. (2006) who analyzed almost the same period in great detail.

The TKE model is run with four different combinations of  $c_h$  and  $c_p$  as defined in Table 1. For  $c_h$  the value of 0.13 was chosen because this predicts  $\phi_{m,h} = 5\zeta$  for  $c_p = 0$  in the stable limit. The current operational value for  $c_h$  is 0.2. For Case D no analytical stable limit solution exists. From the model output we will diagnose flux–gradient relations (and stability functions) and compare the scaling behaviour of our model with the more advanced model of Nieuwstadt (1984). Finally some quantities related to the boundary-layer structure will be investigated. Table 2 summarizes all obtained stable limit solutions for the four defined cases.

#### 5.1 Flux–Gradient Relations

Figure 3 shows flux–gradient relations for the four different combinations of  $c_h$  and  $c_p$  defined in Table 1. Apart from case D, for which no analytical solution exists, in all cases the  $\phi$  functions approach the predicted stable limit (Table 2). For increasing  $c_h$  the  $\phi$  functions become less steep, increasing  $c_p$  causes  $\phi_m$  and  $\phi_h$  to diverge. Obviously, for a near-neutral stratification the  $\phi$  functions deviate from the stable limit solution and the neutral length

**Table 1** Characteristics of the four model runs

	$c_h$	$c_p$	Remarks
A	0.13	0	No Pr dependency; $\phi_m = \phi_h = 5\zeta$ in the stable limit
B	0.13	1	$Pr = 1 + Ri_g$
C	0.2	1	Current operational values
D	0.2	2	No analytical solution

**Table 2** Stable limit solutions for the model runs A, B and C defined Table 1

	A	B	C	N84
$\phi_m/\zeta$	5.0	4.0	1.8	
$\phi_h/\zeta$	5.0	5.4	4.1	
$Ri_g$	0.20	0.33	1.29	0.218
$(2E)^{1/2}/u_*$	2.59	2.54	2.23	2.8
$K_m/(Lu_*)$	0.08	0.10	0.22	0.08
$K_h/(Lu_*)$	0.08	0.07	0.10	0.08

Case D has no analytical solution. For comparison, values for the N84 model are added

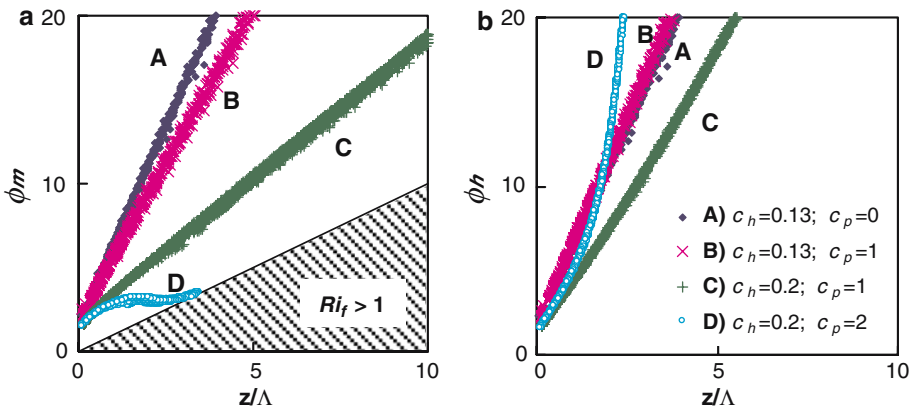


**Fig. 3** Flux–gradient relationships for momentum (a) and heat (b) as diagnosed from model output for four different combinations of  $c_h$  and  $c_p$

scale forces them to be 1. When  $\zeta$  becomes larger than about 1.5, the influence of the neutral length scale becomes very small.

A comparison with  $\phi$  functions from the literature (see Fig. 1) shows that for  $\zeta < 1$  the observations correspond best with cases A and B. However, experimentally obtained flux–gradient relations tend to level off for larger stabilities as for example the D91 and the BH91 functions (Fig. 1). Consequently, for increasing  $\zeta$  the cases A and B deviate from observed values. When stratification is very strong, case C is closest to the observations.

For case D no analytical stable limit solution exists. Figure 3 shows that in this case  $\phi_m$  increases only very slowly and that the increase in  $\phi_h$  is more than linear with stability, which does not agree with observations. Surprisingly, comparison with Fig. 1 shows that this behaviour is well comparable to the rLTG functions. In fact, from Eqs. 9 and 10 it can

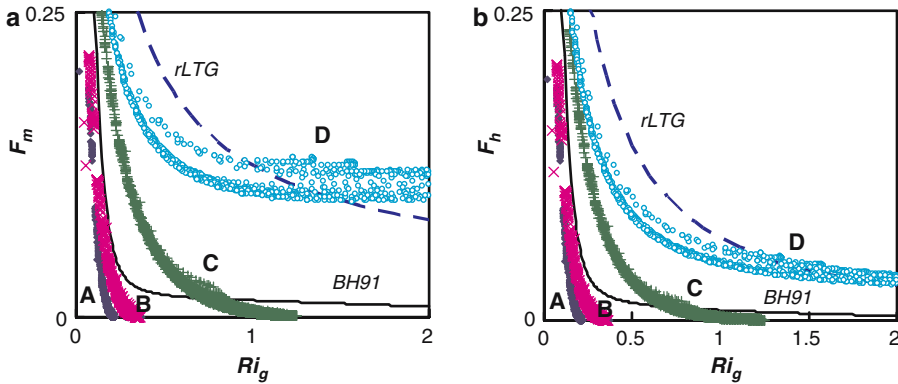


**Fig. 4** Stability functions for momentum (a) and heat (b) for the different model simulations A–D defined in Table 1. For comparison two proposals from the literature are added: the dashed line represents the revised LTG functions, the solid line the Beljaars–Holtslag (1991) functions

be shown that a more than linear increase of  $\phi_h(\zeta)$  is inevitable when one wants to fulfil  $Ri_f < 1$  and at the same time let  $Ri_g \rightarrow \infty$  in the stable limit.

### 5.2 Stability Functions

Stability functions for momentum and heat are given in Fig. 4. The model simulations with low  $c_h$  (0.13) have a low critical  $Ri_g$ , above which all turbulence is switched off. They are well comparable with the BH91 functions, in the sense that mixing decreases rapidly with increasing  $Ri_g$ . Note that the BH91 functions were formulated in such a way that no critical  $Ri_g$  exists. For case C mixing is suppressed more slowly, but still a critical  $Ri_g$  exists at about 1.3. The fact that for case D no stable limit solution exists is consistent with the lack of a critical  $Ri_g$ . The stability functions for this case are comparable with the rLTG functions, thus showing characteristics of ‘enhanced mixing’. As such, case D is not expected to give realistic results in terms of stable boundary-layer structure.

### 5.3 Comparison with the Nieuwstadt (1984) (N84) Model

In this Section we compare the scaling behaviour of our model with the N84 model, which is a full second-order model. N84 applies a slightly different formulation for the stable length scale; instead of  $E^{1/2}$  as in our model the standard deviation of the vertical velocity fluctuation,  $\sigma_w$  is used:

$$l_B = C_B \frac{\sigma_w}{N}, \tag{31}$$

(N84, his Eq. 20), where  $C_B = 1.69$  is a constant. According to his Figs. 2 and 3,  $\sigma_w$  and  $E^{1/2}$  (both scaled by  $u_*$ ) are almost constant as a function of  $\zeta$ . This means that  $\sigma_w$  is a fixed fraction of  $E^{1/2}$ , which implies that the length scales in the two models are equivalent. In fact, for stable conditions our TKE scheme can be considered a reduced version of the N84 model. By reproducing some figures from N84 we will now compare the scaling behaviour of the two models to assess how this behaviour is affected by the simplifications in the TKE-closure approach. The theory of local scaling predicts that dimensionless quantities reach a constant

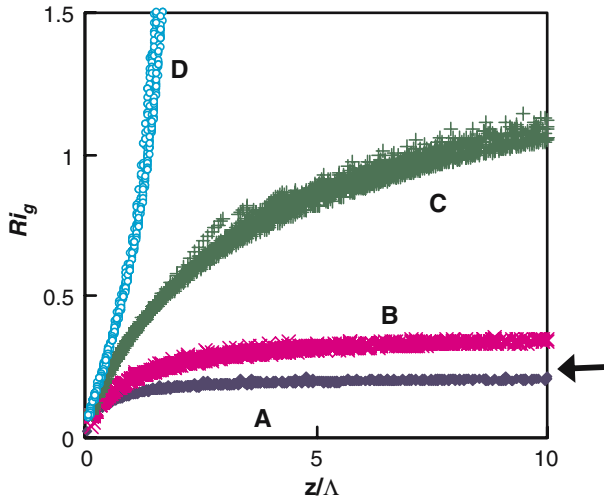


**Fig. 5**  $Ri_g$  vs.  $z/\Lambda$  for the different model simulations A–D defined in Table 1. The stable limit solutions for each case are given in Table 2. The arrow indicates the limit solution of the N84 model

value in the stable limit (N84). In the following figures and in Table 2 the limit of the N84 is given together with the model results for the four runs described above.

Figure 5 (N84, Fig. 9) gives the results for  $Ri_g$  versus  $z/\Lambda$ , and shows that case D does not have a critical  $Ri_g$ , thus violating the theory of local scaling. The other three model runs approach their critical value as predicted by Eq. 30. In the stable limit, Case A is very close to the N84 solution.

The same pattern can be seen in Fig. 6, where the TKE, nondimensionalized by  $u_*$ , is plotted versus stability. Values are constant over the whole stable range, implying that the shear stress is proportional to the TKE everywhere in the stable boundary layer, which is not surprising since in stable conditions shear is the only source of turbulence (N84). The larger  $c_p$ , the lower the equilibrium value that is obtained, though Case D does not reach equilibrium. Stable limit solutions can be calculated according to

$$\frac{\sqrt{2E}}{u_*} = \frac{\sqrt{2}Ri_g^{0.25}}{\sqrt{c_h(1 + c_p Ri_g)}}, \tag{32}$$

which follows directly from  $u_*^2 = K_m S = c_h(1 + c_p Ri_g)EN^{-1}S$ . For  $Ri_g$  Eq. 30 can be used. The scaled eddy diffusivities are given in Fig. 7. Except for Case D, all curves show a gradual increase from zero in neutral conditions to a constant value in the stable limit. The N84 stable limit compares well to our cases A and B, and the stable limit solutions can be obtained from

$$\frac{K_m}{Lu_*} = \frac{k Ri_g}{Pr} = k \frac{\zeta}{\phi_m} \tag{33}$$

and,

$$\frac{K_h}{Lu_*} = \frac{k Ri_g}{Pr^2} = k \frac{\zeta}{\phi_h} \tag{34}$$

and using Eqs. 26 and 27.

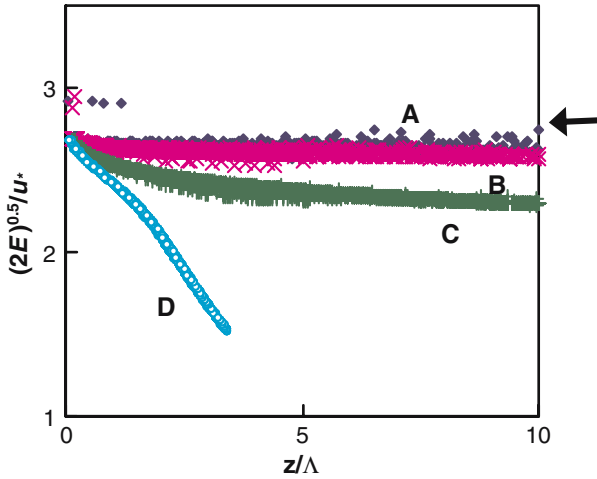


**Fig. 6** TKE, nondimensionalized with  $u_*$  for the different model simulations A–D defined in Table 1. The stable limit solutions for each case are given in Table 2. The arrow indicates the limit solution of the N84 model

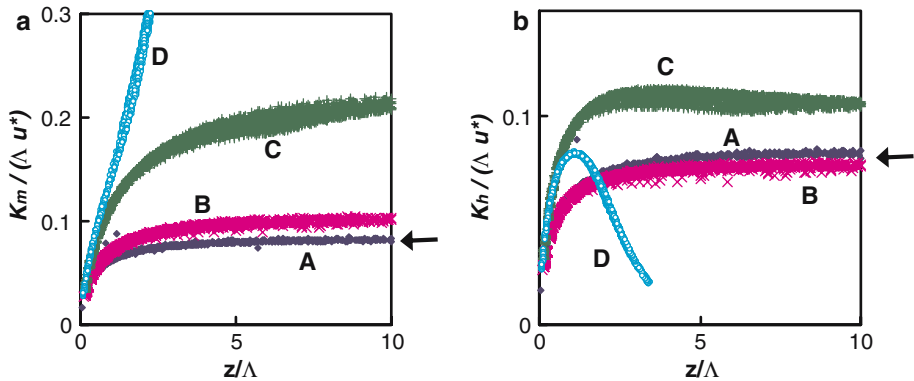


**Fig. 7**  $K_m$  (a) and  $K_h$  (b), both nondimensionalized with  $(\Lambda u_*)$  for the different model simulations A–D defined in Table 1. The stable limit solutions for each case are given in Table 2. The arrow indicates the limit solution of the N84 model. Note the difference in scale on the y-axis

Thus the TKE- $l$  model generates a scaling behaviour comparable to the more advanced N84 model. The stable limits of the N84 model show most agreement with our Case A, which has a relatively low value of  $c_h$  and has  $c_p = 0$ .

### 5.4 Boundary-Layer Structure

So far we have only discussed the scaling behaviour of the model. To demonstrate how the different model simulations represent the boundary-layer structure, we now discuss the boundary-layer height (Fig. 8) and the vertical profiles of the wind speed (Fig. 9). The boundary-layer height,  $h$ , is defined as the level at which the TKE has fallen to 5% of its surface value, divided by 0.95 (as in Cuxart et al. 2006). Model runs A and B produce very shallow boundary layers of less than 100 m during nighttime, combined with a distinct

**Fig. 8** Time series of boundary-layer heights,  $h$ , for the model runs A–D. Crosses indicate sodar retrievals made during the CASES-99 campaign

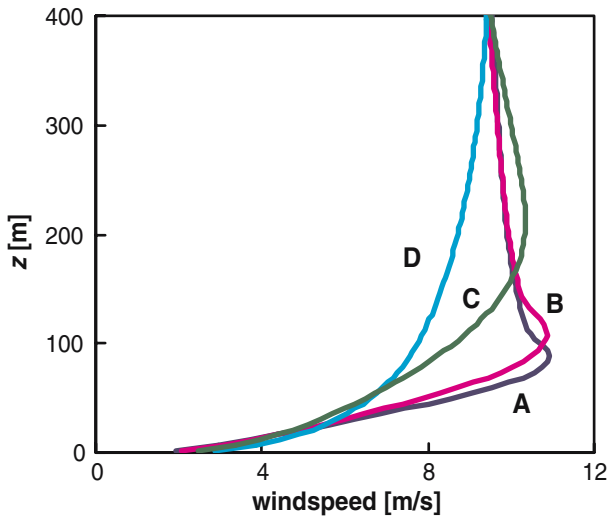
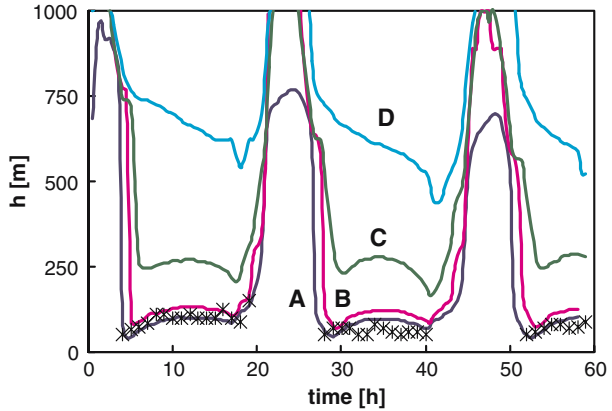


**Fig. 9** Vertical wind profiles at 38 h of simulation (halfway the second night). Letters indicate the model runs A–D

low-level jet. This is in good agreement with sodar retrievals obtained during the CASES-99 campaign. The difference between cases B and C demonstrates the impact of increasing  $c_h$  from 0.13 to 0.2:  $h$  becomes too large compared to observations and the low-level jet becomes much weaker. In case D,  $h$  is far too large and the low-level jet has disappeared. These results are consistent with our earlier finding that case D shows Louis-type stability functions. The corresponding deterioration of the boundary-layer structure is a logical consequence.

### 6 Discussion

Our TKE scheme follows the local scaling hypotheses: for  $z/\Lambda \rightarrow \infty$  dimensionless quantities reach a constant value and the  $\phi$  functions become linear ( $z$ -less scaling). The latter is a direct consequence of  $Ri_f$  and  $Ri_g$  becoming constant. However, as mentioned in Sect. 2, data from experiments show that the  $\phi$  functions level-off for large stabilities. In this Section

we discuss this discrepancy. We further noticed that the ‘imaginary’ case D shows erratic scaling behaviour. Here we discuss how to interpret these results.

To confirm that our results do not depend on boundary conditions we performed sensitivity runs with half the geostrophic forcing and an unrealistic step-wise surface temperature forcing [one at night (4°C), one during daytime (14°C)]. For the different cases we obtained similar results as before (not shown). Apparently, changing the boundary conditions does not influence the scaling behaviour of the scheme, which indicates that this is robust and depends only on model parameters.

### 6.1 The Validity of the Local Scaling Hypotheses

For continuous turbulence the critical  $Ri_f$  is about 0.2 (Beljaars and Holtslag 1991; N84), which is consistent with the relation  $\phi_m = 1 + 5\zeta$ . However, when stability becomes so large that turbulence becomes intermittent,  $Ri_f$  can be larger (Kondo et al. 1978). Assuming that  $\phi_m = 1 + 5\zeta$  is valid for about  $\zeta < 1$ , this implies a levelling off of  $\phi_m$  for larger stabilities. In these conditions the local scaling hypothesis is not valid anymore. Basu et al. (2006) confirm this by showing that mesoscale motions and intermittent turbulence can invalidate local scaling. Mahrt et al. (1998) state that local scaling does not work for  $\zeta > 1$ , which they define as the very stable regime. In fact, this may even explain the difference between the flux–gradient relations found by BH91 and D91 (Fig. 1). The D91 functions were based on N84 who selected only data with a wind speed of more than  $5 \text{ m s}^{-1}$  to avoid intermittent turbulence as much as possible. Consequently, the D91 functions level off much slower than the BH91 functions that do not make this selection. Since our TKE scheme strictly follows local scaling theory it is not surprising that the model does not reproduce the levelling off of the flux–gradient relations for large  $\zeta$ . From a practical point of view it may be questioned whether this levelling off effect is important, because for such strongly stable conditions turbulent fluxes are very small anyway and radiative processes may dominate the energy balance (André and Mahrt 1982). In addition, the results for the GABLS case are good when using parameter setting A or B, whereas they deteriorate using the enhanced mixing in cases C and D. This indicates that a realistic behaviour of the  $\phi$  functions for  $\zeta < 1$  is crucial.

### 6.2 Understanding the Output of Case D

In Sect. 4 we concluded that for certain combinations of  $c_h$  and  $c_p$  no stationary solution is possible. By running the model with such a ‘forbidden’ combination we found that the scaling behaviour of the model becomes unrealistic as in case D. Even under these conditions model results shows that the transport of TKE plays a minor role. In this case the equations prohibit the model to reach a steady state. Instead,  $E$  grows every timestep and so do  $l_m$ ,  $Ri_g$  and  $K_m$ . This process continues until  $l_m$  becomes limited by its neutral part (see Eq. 14). Alternatively,  $c_m$  can be maximized artificially by e.g.  $c_m = c_h[\max(1 + 2Ri_g, 4)]$ . In this case the stable limits can be easily calculated by using  $c_h$  and  $c_m = 4c_h$  in Eqs. 21 and 22. Of course other dependencies of  $c_m$  on  $c_h$  can be tested, as done by Tijn (2004) for example.

As shown in Sect. 5, results for case D seem to represent rLTG type of diffusion. Therefore, it might be tempting to apply comparable parameter settings if implementation of TKE closure with strong diffusion is desirable. However, we do not recommend this. In our opinion introducing more advanced physics (i.c. TKE closure) and deliberately maintaining the mixing under stably stratified conditions unrealistically high (in order to improve other aspects of the model, e.g. the large-scale atmospheric dynamics) should be avoided. Instead, implementation of TKE closure in operational models should lead to a more realistic SBL structure,

suggesting a value for  $c_h$  of about 0.13 and a rather small value of  $c_p$ . Matching the observed mixing characteristics in the SBL with the highly diffusive boundary layers apparently needed in a NWP model needs clearly more research.

## 7 Conclusions

TKE turbulence closure is increasingly applied in research numerical atmosphere models, but most large-scale operational models still apply first-order closure. One of the reasons is that uncertainties exist in the scaling behaviour of TKE models and that it is questioned whether this behaviour can be controlled.

We studied the scaling behaviour of a TKE model for stably stratified conditions. The length scale for stable conditions is proportional to the ratio of the square root of the TKE and the local Brunt–Väisälä frequency, which is a commonly used formulation (Deardorff 1980). The scaling behaviour of the model for stably stratified conditions is controlled by the constants of proportionality preceding this ratio. Motivated by observations and 3D model performance, the turbulent Prandtl number can be expressed as a function of stability. As a prototype we used  $Pr = 1 + c_p Ri_g$ . From the model equations we analyzed expressions for the stable limit of various scaling quantities such as the flux–gradient relations.

Obviously, the generality of our results can be questioned, since we investigated only a single model. However, we note that the Deardorff length scale is a rather common formulation in TKE closures, and that some other proposals [e.g. the parcel method developed by Bougeault and Lacarrère (1989)] reduce to the Deardorff length scale in stable conditions as well. We believe that our results have a general applicability for such models. We also acknowledge that they are not generally valid for all other length scale proposals found in the literature, but our results may act to stimulate similar analyses for those schemes. The current function which allows  $Pr$  to vary with stability is less frequently applied. Yet, our results show that the inclusion of such an empirical correction function may have large and undesired consequences for the model behaviour (in our case an inability to obtain a steady state with the Deardorff length scale, and drift to a state that is dominated by the limiting neutral length scale).

Depending on parameter choice, different regimes can be distinguished in the scaling behaviour of our model. In the first regime the model follows the local scaling theory of Nieuwstadt (1984), which can be considered as an extension of the surface based Monin–Obukhov Similarity Theory: in the stable limit dimensionless parameters become constant and the flux–gradient relations become linear ( $z$ -less scaling). However, most observational studies show the flux–gradient relations leveling off for very strong stratification. This is probably due to the fact that under these conditions turbulence loses its continuous character, thereby violating basic assumptions underlying the theory of local scaling.

In the second regime the scaling behaviour of the model becomes unrealistic and violates local scaling theory. This occurs when, depending on the mixing efficiency for heat,  $c_p$  is taken larger than a certain threshold value. In this regime, no stationary solution of the TKE equation is possible: the shear production becomes so large that the buoyancy destruction and the dissipation can no longer balance the TKE equation anymore. Surprisingly, the stability functions now resemble the formulations that are currently used by large-scale operational models as e.g. the Louis functions of the ECMWF model. We do not recommend implementing this type of enhanced mixing in a TKE closure model. In our opinion the introduction of a TKE scheme should aim for realistic mixing characteristics leading to a more accurate representation of the SBL structure.

The analytical results were illustrated by four model simulations with different mixing characteristics. Sensitivity runs were done to investigate whether the obtained scaling behaviour was not just an artefact of the selected case study or the model details. It turned out that changing the boundary conditions and the vertical resolution did not affect the scaling results. The correspondence between our results and those of the full second-order model of Nieuwstadt (1984) model is good. This shows that simplifications made in the TKE-closure approach have little impact for the stable boundary-layer scaling behaviour.

**Acknowledgements** We acknowledge Bert Holtslag and Gert-Jan Steeneveld from Wageningen University as well as three anonymous reviewers for their valuable comments on the manuscript. The first author has been supported by the Netherlands Organization for Scientific Research (NWO), in particular through the project “land surface climate and the role of the stable boundary layer”. In addition part of this research was carried out in the framework of the Dutch National Research Program “climate changes spatial planning” (<http://www.klimaatvoornuimte.nl>).

## References

- André JC, Mahrt L (1982) The nocturnal surface inversion and influence of clear-air radiative cooling. *J Atmos Sci* 39:864–878
- Andreas EL (2002) Parameterizing scalar transfer over snow and ice: a review. *J Hydrometeorol* 3:417–432
- Baas P, Steeneveld GJ, van de Wiel BJH, Holtslag AAM (2006) Exploring self-correlation in flux–gradient relationships for stably stratified conditions. *J Atmos Sci* 63:3045–3054
- Basu S, Begum ZN, Rajagopal EN (1998) Impact of boundary-layer parameterization schemes on the prediction of the Asian summer monsoon. *Boundary-Layer Meteorol* 86:469–485
- Basu S, Porté-Agel F, Foufoula-Georgiou E, Vinuesa JF, Pahlow M (2006) Revisiting the local scaling hypothesis in stably stratified atmospheric boundary-layer turbulence: an integration of field and laboratory measurements with large-eddy simulations. *Boundary-Layer Meteorol* 119:473–500
- Beljaars ACM, Holtslag AAM (1991) Flux parameterization over land surfaces for atmospheric models. *J Appl Meteorol* 30:327–341
- Beljaars ACM, Viterbo P (1998) Role of the boundary layer in a numerical weather prediction model. In: Holtslag AAM, Duynkerke PG (eds) Clear and cloudy boundary layers. Royal Netherlands Academy of Arts and Sciences, Amsterdam, pp 287–304
- Bertin F, Barat J, Wilson R (1997) Energy dissipation rates, eddy-diffusivity, and the Prandtl number: an in situ experimental approach and its consequences on radar estimate of turbulent parameters. *Radio Sci* 32:791–804
- Bougeault P, Lacarrère P (1989) Parameterization of orography-induced turbulence in a mesobeta-scale model. *Mon Wea Rev* 117:1872–1890
- Brinkop S, Roeckner E (1995) Sensitivity of a general circulation model to parameterizations of cloud-turbulence interactions in the atmospheric boundary layer. *Tellus* 47A:197–220
- Businger JA, Wyngaard JC, Izumi Y, Bradley EF (1971) Flux profile relationships in the atmospheric surface layer. *J Atmos Sci* 28:181–189
- Canuto VM, Howard AM, Cheng Y, Dubovikov MS (2001) Ocean turbulence. Part I: one-point closure – momentum and heat vertical diffusivities. *J Phys Oceanogr* 31:1413–1426
- Cheinet S, Beljaars A, Köhler M, Morcrette JJ, Viterbo P (2005) Assessing physical processes in the ECMWF model forecasts using ARM SGP observations. In: ARM report series no. 1. ECMWF, U.K., 25 pp
- Cheng Y, Canuto VM, Howard AM (2002) An improved model for the turbulent PBL. *J Atmos Sci* 59:1550–1565
- Cheng Y, Parlange MB, Brutsaert W (2005) Pathology of Monin–Obukhov similarity in the stable boundary layer. *J Geophys Res* 110:D06101
- Chimonas C, Nappo CJ (1989) Wave drag in the planetary boundary layer over complex terrain. *Boundary-Layer Meteorol* 47: 217–232
- Cuxart J, Bougeault P, Redelsperger JL (2000) A turbulence scheme allowing for mesoscale and large-eddy simulations. *Quart J Roy Meteorol Soc* 126:1–30
- Cuxart J, Morales G, Terradellas E, Yagüe C (2002) Study of coherent structures and estimation of the pressure transport terms for the nocturnal stable boundary layer. *Boundary-Layer Meteorol* 105:305–328

- Cuxart J, Holtslag AAM, Beare RJ, Bazile E, Beljaars A, Cheng A, Conangla L, Ek MB, Freedman F, Hamdi R, Kerstein A, Kitagawa H, Lenderink G, Lewellen D, Mailhot J, Mauritsen T, Perov V, Schayes G, Steeneveld GJ, Svensson G, Taylor P, Weng W, Wunsch S, Xu KM (2006) Single-column model inter-comparison for a stably stratified atmospheric boundary layer. *Boundary-Layer Meteorol* 118:273–303
- Deardorff JW (1980) Stratocumulus-capped mixed layers derived from a three-dimensional model. *Boundary-Layer Meteorol* 18:495–527
- Duynkerke PG (1991) Radiation fog: a comparison of model simulations with detailed observations. *Mon Wea Rev* 119:324–341
- Duynkerke PG, de Roode SR (2001) Surface energy balance and turbulence characteristics observed at the SHEBA ice camp during FIRE III. *J Geophys Res* 106:15313–15322
- Dyer AJ (1974) A review of flux-profile relationships. *Boundary-Layer Meteorol* 7:363–372
- Högström U (1988) Nondimensional wind and temperature profiles in the atmospheric boundary layer. *Boundary-Layer Meteorol* 42:55–78
- Holtslag AAM (1998) Modelling of atmospheric boundary layers. In: Holtslag AAM, Duynkerke PG (eds) *Clear and cloudy boundary layers*. Royal Netherlands Academy of Arts and Sciences, Amsterdam, pp 287–304
- Holtslag AAM (2006) GEWEX atmospheric boundary layer study (GABLS) on stable boundary layers. *Boundary-Layer Meteorol* 118:85–110
- Howell JF, Sun J (1999) Surface-layer fluxes in stable conditions. *Boundary-Layer Meteorol* 90:495–520
- Jones CG, Lenderink G, Ivarsson LI (2003) Representing subgrid scale mixing under stable conditions: importance for overall model synoptic development. *Hirlam Newslett* 43:125–134
- Kim J, Mahrt L (1992) Simple formulation of mixing in the stable free atmosphere and nocturnal boundary layer. *Tellus* 44A:381–394
- Kondo J, Kanechika O, Yasuda N (1978) Heat and momentum transfer under strong stability in the atmospheric surface layer. *J Atmos Sci* 35:1012–1021
- Lenderink G, Holtslag AAM (2000) Evaluation of the kinetic energy approach for modeling turbulent fluxes in stratocumulus. *Mon Wea Rev* 128:244–258
- Lenderink G, Holtslag AAM (2004) An updated length scale formulation for turbulent mixing in clear and cloudy boundary layers. *Quart J Roy Meteorol Soc* 130:3405–3427
- Lenderink G, van den Hurk B, van Meijgaard E, van Ulden A, Cuijpers H (2003) Simulation of present-day climate in RACMO2: first results and model development. In: TR-252. KNMI, The Netherlands, 24 pp
- Lenderink G, Siebesma AP, Cheinet S, Irons S, Jones CG, Marquet P, Mueller F, Olmeda D, Calvo J, Sanchez E, Soares PMM (2004) The diurnal cycle of shallow cumulus clouds over land: A single column model intercomparison study. *Quart J Roy Meteorol Soc* 130:3339–3364
- Lock A, Mailhot J (2006) Combining non-local scalings with a TKE closure for mixing in boundary layer clouds. *Boundary-Layer Meteorol* 121:313–338
- Louis JF, Tiedtke M, Geleyn JF (1982) A short history of the PBL parameterization at ECMWF. In: *Workshop on boundary layer parameterization*. ECMWF, UK, pp 59–79
- Mahrt L (1987) Grid-averaged surface fluxes. *Mon Wea Rev* 115:1550–1560
- Mahrt L (2007) The influence of nonstationarity on the turbulent flux-gradient relationship for stable stratification. *Boundary-Layer Meteorol* 125:245–264
- Mahrt L, Sun J, Blumen W, Delany W, Oncley S (1998) Nocturnal boundary layer regimes. *Boundary-Layer Meteorol* 88:255–278
- Mailot J, Benoit R (1982) A finite-element model of the atmospheric boundary layer suitable for use with numerical weather prediction models. *J Atmos Sci* 39:2249–2266
- Mauritsen T, Svensson G (2007) Observations of stably stratified shear-driven atmospheric turbulence at low and high Richardson numbers. *J Atmos Sci* 64:645–655
- McCabe A, Brown AR (2007) The role of surface heterogeneity in modeling the stable boundary layer. *Boundary-Layer Meteorol* 122:517–534
- Mellor GL, Yamada T (1974) A hierarchy of turbulence closure models for planetary boundary layers. *J Atmos Sci* 31:1791–1806
- Nieuwstadt FTM (1984) The turbulent structure of the stable, nocturnal boundary layer. *J Atmos Sci* 41:2202–2216
- Poulos GS, Blumen W, Fritts DC, Lundquist JK, Sun J, Burns SP, Nappo C, Banta R, Newsom R, Cuxart J, Terradellas E, Balsley B, Jensen M (2002) CASES-99: a comprehensive investigation of the stable nocturnal boundary layer. *Bull Am Meteorol Soc* 83:555–581
- Schumann U, Gerz T (1995) Turbulent mixing in stably stratified shear flows. *J Appl Meteorol* 34:33–48
- Steenefeld GJ, van de Wiel BJH, Holtslag AAM (2006) Modeling the evolution of the atmospheric boundary layer for three contrasting nights in CASES-99. *J Atmos Sci* 63:920–935

- Steeneveld GJ, Mauritsen T, de Bruijn EIF, Vila-Guerau de Arellano J, Svensson G, Holtslag AAM (2007) Evaluation of limited area models for the representation of the diurnal cycle and contrasting nights in CASES99. *J Appl Meteorol Clim* (in press)
- Stull RB (1988) *An introduction to boundary layer meteorology*. Kluwer Academic Publishers, Dordrecht, The Netherlands, 666 pp
- Svensson G, Holtslag AAM (2006) Single column modeling of the diurnal cycle based on CASES99 data – GABLS second intercomparison project. In: 17th symposium on boundary layers and turbulence, San Diego, CA, USA, 22–25 May 2006. Amer. Meteorol. Soc., Boston, p 8.1
- Tijm ABC (2004) Tuning CBR. *Hirlam Newslett* 46:18–28
- Umlauf L, Burchard H (2005) Second-order turbulence closure models for geophysical boundary layers. A review of recent work. *Cont Shelf Res* 25:795–827
- Viterbo P, Beljaars ACM, Mahfouf JF, Teixeira J (1999) The representation of soil moisture freezing and its impact on the stable boundary layer. *Quart J Roy Meteorol Soc* 125:2401–2426
- Weng W, Taylor PA (2003) On modelling the one-dimensional atmospheric boundary layer. *Boundary-Layer Meteorol* 107:371–400
- Wyngaard JC, Coté OR (1974) The evolution of a convective planetary boundary layer – a higher-order-closure model study. *Boundary-Layer Meteorol* 7:289–308
- Zilitinkevich SS, Esau IN (2007) Similarity theory and calculation of turbulent fluxes at the surface for the stably stratified atmospheric boundary layer. *Boundary-Layer Meteorol* 125:193–205
- Zilitinkevich SS, Elperin T, Kleorin N, Rogachevskii I (2007) Energy- and flux-budget (EFB) turbulence closure model for stably stratified flows. Part I: steady-state, homogeneous regimes. *Boundary-Layer Meteorol* 125:167–191